

Doping optimization of organic-inorganic hybrid perovskite $\text{CH}_3\text{NH}_3\text{PbI}_3$ for high thermoelectric efficiency



Tianqi Zhao^a, Dong Wang^{a,*}, Zhigang Shuai^{a,b,**}

^a MOE Key Laboratory of Organic OptoElectronics and Molecular Engineering, Department of Chemistry, Tsinghua University, Beijing 100084, PR China

^b Key Laboratory of Organic Solids, Beijing National Laboratory for Molecular Science (BNLMS), Institute of Chemistry, Chinese Academy of Sciences, Beijing 100190, PR China

ARTICLE INFO

Article history:

Received 22 September 2016

Received in revised form 7 December 2016

Accepted 9 January 2017

Available online 19 January 2017

Keywords:

Organic-inorganic hybrid perovskite

Thermoelectric transport

First-principles calculations

ABSTRACT

The newly discovered photovoltaic hybrid perovskite materials have been suggested for thermoelectric applications as they possess very low thermal conductivity and large Seebeck coefficient. However, to achieve a high figure of merit, chemical doping is necessary to increase the electrical conductivity. In the present work, we examined the thermoelectric figure of merit for $\text{CH}_3\text{NH}_3\text{PbI}_3$ as a function of carrier concentration based on first-principles calculations. For doped semiconductors, the impurity scattering usually plays a dominant role in the charge transport. Both impurity scattering and acoustic phonon scattering have been incorporated in our calculations. We showed that at the impurity concentration of 10^{18} cm^{-3} , the room temperature zT value of tetragonal $\text{CH}_3\text{NH}_3\text{PbI}_3$ could be optimized to reach unity at the carrier concentration on the same order of magnitude as 10^{18} cm^{-3} . The hole-doped $\text{CH}_3\text{NH}_3\text{PbI}_3$ exhibits superior thermoelectric property than the electron-doped one, and we propose to engineer the vacancies of organic cations for the enhanced hole concentration and thermoelectric efficiency.

© 2017 Elsevier B.V. All rights reserved.

1. Introduction

Thermoelectric (TE) materials provide a direct energy conversion scenario between heat and electricity, and have attracted intensive interests for their potential applications in waste heat recycle and space power generation [1–3]. The efficiency of a TE material is characterized by the dimensionless figure of merit zT , defined as $zT = \frac{S^2\sigma T}{\kappa}$, where S , σ , T , and κ are Seebeck coefficient, electrical conductivity, temperature and thermal conductivity, respectively. The thermal conductivity is constituted by two parts, the electrical thermal conductivity (κ_e) and the lattice thermal conductivity (κ_l). High performance TE materials should possess high Seebeck coefficient and electrical conductivity as well as low thermal conductivity, i.e., the electrical transport properties should be enhanced but the phonon transport should be suppressed.

To compete with other renewable energy solutions, zT is expected to exceed 1.5 for the entire relevant temperature range. Among bulk inorganic TE materials, the commercialized bismuth telluride based alloys possess zT around one [4,5]. The newly reported SnSe single crystal possesses zT ranging from 0.7 to 2.0 in the temperature range of 300–773 K, which is mainly ascribed to the enhanced Seebeck coefficient and high electrical conductivity achieved by hole doping [6]. However, the cost of inorganic TE modules per watt for power generation, cooling, or heating is so high as to have limited their applications [7]. As compared to inorganic materials, organic materials are low-cost, solution processable, and flexible. Organic TE materials have low thermal conductivity, but their electrical properties are poor, often leading to very low energy conversion efficiency. The best known organic TE materials are conducting polymers, particularly PEDOT:Tos and PEDOT:PSS. Lab researches show that the zT value of p-type PEDOT has achieved 0.2–0.5 by doping engineering [8,9], and that of n-type metal coordination polymer poly(nickel-ethylenetetra-thiolate) has reached 0.30 at room temperature [10].

Organic-inorganic composite materials have the potential to combine the advantages of their organic and inorganic constituents, i.e., poor thermal transport in the organic component, and excellent charge transport in the inorganic component. However, how to process such composite materials to achieve the best TE

* Corresponding author.

** Corresponding author at: MOE Key Laboratory of Organic OptoElectronics and Molecular Engineering, Department of Chemistry, Tsinghua University, Beijing 100084, PR China.

E-mail addresses: dong913@tsinghua.edu.cn (D. Wang), zgshuai@tsinghua.edu.cn (Z. Shuai).

performance is yet to be explored. Recently, organic anions have been intercalated in layered transition metal dichalcogenide TiS_2 to fabricate the hybrid, which possesses a zT value of 0.28 at 373 K [11]. It was shown that the organic intercalation causes a significant reduction of the thermal conductivity, while the hybrid retains the high electrical power factor of TiS_2 . The newly discovered organic-inorganic hybrid perovskite materials are originally used as sensitizers in photovoltaics [12]. Afterwards, it has been demonstrated with a planar heterojunction solar cell device structure [13], and the photo conversion efficiency reaches 22.1% [14]. The great success of $\text{CH}_3\text{NH}_3\text{PbI}_3$ in photovoltaics can be largely ascribed to its excellent optical absorption, high carrier mobility and long diffusion length of charge carriers. Though $\text{CH}_3\text{NH}_3\text{PbI}_3$ has a low formation energy and suffers from the poor stability in moisture and air, progress has been made to improve the stability of perovskite solar cells against water and oxygen degradation [15–18]. $\text{CH}_3\text{NH}_3\text{PbI}_3$ has also been reported to have an ultralow thermal conductivity ($0.59 \text{ W m}^{-1} \text{ K}^{-1}$ at room temperature) [19,20]. These properties have inspired great interests in $\text{CH}_3\text{NH}_3\text{PbI}_3$ for solar TE applications [21–23]. We noted that the TE figure of merit for $\text{CH}_3\text{NH}_3\text{PbI}_3$ has been studied from first-principles calculations [22,23]. In Ref. [22], He and Galli only accounted for the acoustic phonon scattering of charge carriers in the calculation of electrical transport properties, while in Ref. [23], the TE properties were calculated by solving the Boltzmann transport equation under the constant relaxation time approximation, and the relaxation time was supplied as an empirical parameter. We have shown in our previous works that when only the acoustic phonon scattering is taken into account, the charge carrier mobility and the zT value would be over-estimated [24,25]. We found that in PEDOT:Tos after the ionized impurity scattering process was included to account for the doping effect, the calculated TE transport coefficients were in reasonable agreement with the available experimental data [24]. Indeed, for TE applications, doping is an effective way to enhance power factors, so the ionized impurity scattering becomes an important scattering mechanism of charge carriers that needs to be considered to give good evaluations of TE properties. Our earlier study of the charge carrier mobility in $\text{CH}_3\text{NH}_3\text{PbI}_3$ perovskite showed that the ionized impurity scattering dominates over the acoustic phonon scattering when the density of impurity reaches 10^{18} cm^{-3} [26].

Herein we investigate the TE transport properties of $\text{CH}_3\text{NH}_3\text{PbI}_3$ by using the Boltzmann transport theory in the relaxation time approximation, and incorporating both acoustic phonon scattering and ionized impurity scattering mechanisms. We find that the TE performance of tetragonal $\text{CH}_3\text{NH}_3\text{PbI}_3$ is better than that of the cubic one due to the higher carrier mobility and the lower thermal conductivity in the tetragonal phase. The p-type $\text{CH}_3\text{NH}_3\text{PbI}_3$ perovskite has higher figure of merit than the n-type one, and the p-type tetragonal $\text{CH}_3\text{NH}_3\text{PbI}_3$ can achieve the highest zT value of 1.26 at the phase transition temperature of 330 K at the carrier density of $6 \times 10^{18} \text{ cm}^{-3}$. The hole doping by the accurate control of the vacancy density of organic cations is suggested. Our theoretical predictions may act as a guide in the doping optimization of the TE performance of $\text{CH}_3\text{NH}_3\text{PbI}_3$ perovskites.

2. Methodological approach

2.1. Electronic structure calculations

The electronic structure calculations were performed within the framework of density functional theory (DFT), using the projector augmented wave (PAW) method as implemented in the Vienna Ab initio Simulation Package (VASP) [27,28] for both cubic

and tetragonal phases of $\text{CH}_3\text{NH}_3\text{PbI}_3$ perovskites. The Perdew-Burke-Ernzerhof (PBE) [29] exchange-correlation functional and the generalized gradient approximation (GGA) were adopted. The spin-orbit coupling (SOC) effect was included in all the calculations for the presence of heavy element lead. A \mathbf{k} -mesh of $4 \times 4 \times 4$ was used to optimize the lattice parameters and atomic positions until the forces on each atom were less than 0.01 eV \AA^{-1} . The energy convergence criterion in the self-consistent field iteration was 10^{-5} eV . The converged charge density was obtained on a \mathbf{k} -mesh of $7 \times 7 \times 7$ and $9 \times 9 \times 9$ for tetragonal and cubic $\text{CH}_3\text{NH}_3\text{PbI}_3$, respectively.

2.2. Boltzmann transport theory

The Boltzmann transport equation describes how a single-particle state population function of charge carries evolves as time in the external fields such as weak electric or magnetic field and thermal gradient. By invoking the relaxation time approximation, TE transport parameters, such as electrical conductivity σ , Seebeck coefficient S and electric thermal conductivity κ_e , can be derived by solving the steady-state Boltzmann transport equation [30]:

$$\sigma = \frac{e^2}{\Omega} \int \tau(\mathbf{k}) \mathbf{v}(\mathbf{k}) \mathbf{v}(\mathbf{k}) \left(-\frac{\partial f^0(\varepsilon_{\mathbf{k}})}{\partial \varepsilon_{\mathbf{k}}} \right) d\varepsilon \quad (1)$$

$$\kappa_0 = \frac{1}{\Omega} \int \tau(\mathbf{k}) \mathbf{v}(\mathbf{k}) \mathbf{v}(\mathbf{k}) \frac{(\varepsilon_{\mathbf{k}} - \varepsilon_f)^2}{T} \left(-\frac{\partial f^0(\varepsilon_{\mathbf{k}})}{\partial \varepsilon_{\mathbf{k}}} \right) d\varepsilon \quad (2)$$

$$S = \frac{e}{\sigma T} \int \tau(\mathbf{k}) \mathbf{v}(\mathbf{k}) \mathbf{v}(\mathbf{k}) (\varepsilon_{\mathbf{k}} - \varepsilon_f) \left(-\frac{\partial f^0(\varepsilon_{\mathbf{k}})}{\partial \varepsilon_{\mathbf{k}}} \right) d\varepsilon \quad (3)$$

$$\kappa_e = \kappa_0 - S^2 \sigma T \quad (4)$$

where $\tau(\mathbf{k})$ is the relaxation time of charge carriers, $\mathbf{v}(\mathbf{k})$ is the group velocity, Ω is the volume of unit cell, f^0 is the Fermi-Dirac distribution function, ε_f is the Fermi level, $\varepsilon_{\mathbf{k}}$ is the electronic band eigenvalues, and κ_0 is the thermal tensor. The band energies on a fine \mathbf{k} -mesh of $41 \times 41 \times 41$ for cubic and $31 \times 31 \times 31$ for tetragonal $\text{CH}_3\text{NH}_3\text{PbI}_3$, respectively, were calculated based on the converged charge density, and interpolated on a \mathbf{k} -mesh 10 times denser.

The relaxation time is the inverse of the scattering probability of charge carriers by phonons, impurities and/or defects. The scattering of charge carriers helps to balance the effect of external fields, namely, the deviation of the distribution function from its equilibrium. According to the Mathiessen's rule, if different scattering events are assumed to be independent of each other, the total relaxation time takes the form:

$$\frac{1}{\tau} = \frac{1}{\tau_{ac}} + \frac{1}{\tau_{imp}} \quad (5)$$

where τ_{ac} and τ_{imp} represent relaxation times due to acoustic phonon scattering and impurity scattering, respectively. According to the Fermi's golden rule, the relaxation time can be expressed as:

$$\frac{1}{\tau(\mathbf{k})} = \sum_{\mathbf{k}'} \frac{2\pi}{\hbar} \delta(\varepsilon(\mathbf{k}) - \varepsilon(\mathbf{k}')) |M(\mathbf{k}, \mathbf{k}')|^2 \cdot (1 - \cos\theta) \quad (6)$$

where $|M(\mathbf{k}, \mathbf{k}')|$ is the scattering matrix element describing the scattering process of charge carriers from Bloch state \mathbf{k} to \mathbf{k}' and θ is the corresponding scattering angle.

2.3. Deformation potential theory for acoustic phonon scattering

The deformation potential (DP) theory [31] has been successfully applied to predicting the carrier mobility in graphene, graphdiyne, and organic molecular crystals [32]. The DP theory describes the acoustic phonon scattering in the long-wave limit. The scattering matrix element can be expressed as

$$|M(\mathbf{k}, \mathbf{k}')|^2 = \frac{k_B T E_1^2}{C_{ii}} \quad (7)$$

where E_1 and C_{ii} are deformation potential constant and elastic constant, respectively. Both of them can be easily derived from first-principles calculations. We applied uniaxial strains to the unit cell of $\text{CH}_3\text{NH}_3\text{PbI}_3$ along the three crystal directions, respectively. The elastic constants were obtained by the parabolic fitting of the total energy to the strain, while the deformation potential constants for electrons and holes were obtained by the linear fitting of the conduction and valence band energy shift, respectively, against the strain.

2.4. Brooks-Herring method for ionized impurity scattering

The Brooks-Herring approach [33] was applied to calculate the scattering matrix element of charge carriers by ionized impurity or defects. The interaction takes the form of a screened Coulomb potential

$$V(\mathbf{r}) = \frac{Z_{ion} e^2}{4\pi \epsilon_r \epsilon_0 r} e^{-r/L_D} \quad (8)$$

where Z_{ion} is the charge of the ionized impurity, ϵ_r and ϵ_0 are the relative and vacuum dielectric constant, respectively. The experimental value of $\epsilon_r = 6.5$ [34] was taken in our calculations. L_D is the Debye screening length, $L_D = \sqrt{\epsilon_r \epsilon_0 k_B T / e^2 n}$, where n is the free charge carrier density. The scattering matrix element is

$$|M(\mathbf{k}, \mathbf{k}')|^2 = \frac{n_{imp} Z_{ion}^2 e^4}{\Omega^2 (\epsilon_r \epsilon_0)^2 (L_D^{-2} + |\mathbf{k}' - \mathbf{k}|^2)^2} \quad (9)$$

where n_{imp} is the density of ionized impurity, Ω is the volume of the unit cell. We take Z_{ion} to be one. The ionized impurities are assumed to affect the scattering of charge carriers independently, and the scattering rate is directly proportional to the density of ionized impurities.

3. Results and discussion

3.1. Tuning carrier concentration for high TE figure of merit

The band structure and charge carrier mobilities of cubic and tetragonal $\text{CH}_3\text{NH}_3\text{PbI}_3$ have been calculated in our previous work [26]. Both cubic and tetragonal phases of $\text{CH}_3\text{NH}_3\text{PbI}_3$ are direct band gap semiconductors, but their band gaps are severely underestimated by the SOC-DFT method. In the calculation of charge transport properties, we applied the so-called scissor operator to the conduction band energies to reproduce the experimental band gap of 1.6 eV. The scissor operator does not change the band dispersion and group velocities. When the Fermi level is in the gap and the carrier concentration is low, both conduction and valence bands may contribute to the Seebeck coefficients with opposite signs, resulting in a drop of the Seebeck coefficients at low carrier concentrations. This is known as the bipolar effect. With the underestimated band gap, the bipolar effect would be more pronounced. For this reason, the scissor operator has been widely applied to the conduction band energies to produce the correct carrier concentration dependence of Seebeck coefficients [35,36].

The electrical conductivity, Seebeck coefficient and electronic thermal conductivity all vary with the charge carrier concentration. To tune the carrier type and concentration, we simply shifted the Fermi level towards the conduction or valence band to mimic the n-type or p-type doping, respectively. If the carrier concentration is low, it is safe to assume that the band structures are not influenced by doping. This is known as the rigid band approximation. The electrical conductivity, Seebeck coefficient, electronic thermal conductivity, and power factor as a function of the carrier concentration have been shown in Fig. 1 for tetragonal phase and Fig. 2 for cubic phase at the temperature of 330 K. The hybrid perovskite $\text{CH}_3\text{NH}_3\text{PbI}_3$ undergoes the phase transition at the temperature of 330 K. At the temperature above 330 K it is cubic and below 330 K it is tetragonal. In tetragonal $\text{CH}_3\text{NH}_3\text{PbI}_3$, [100] and [010] are degenerate directions. In cubic phase of $\text{CH}_3\text{NH}_3\text{PbI}_3$, [010] and [001] are degenerate directions. The organic cation CH_3NH_3 lies parallel to the [100] direction, so it becomes pseudocubic after optimization. We only present the data in [100] and [001] directions.

As shown in Figs. 1 and 2, the electrical conductivity increases with the carrier concentration, and the Seebeck coefficient decreases linearly with the logarithm of the carrier concentration.

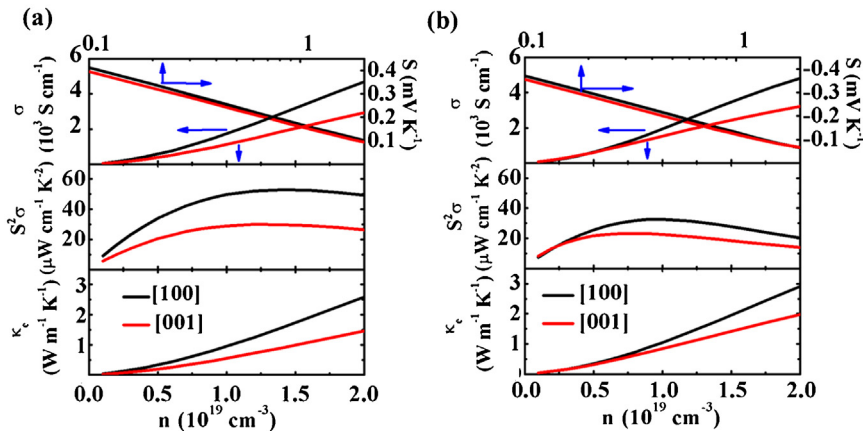


Fig. 1. Electrical conductivity σ , Seebeck coefficient S , power factor $S^2\sigma$, and electronic thermal conductivity κ_e of tetragonal $\text{CH}_3\text{NH}_3\text{PbI}_3$ at 330 K, as a function of hole (a) and electron (b) concentration. The black and red lines represent the [100] and [001] transport directions, respectively. The Seebeck coefficient is positive for holes and negative for electrons. (For interpretation of the references to colour in this figure legend, the reader is referred to the web version of this article.)

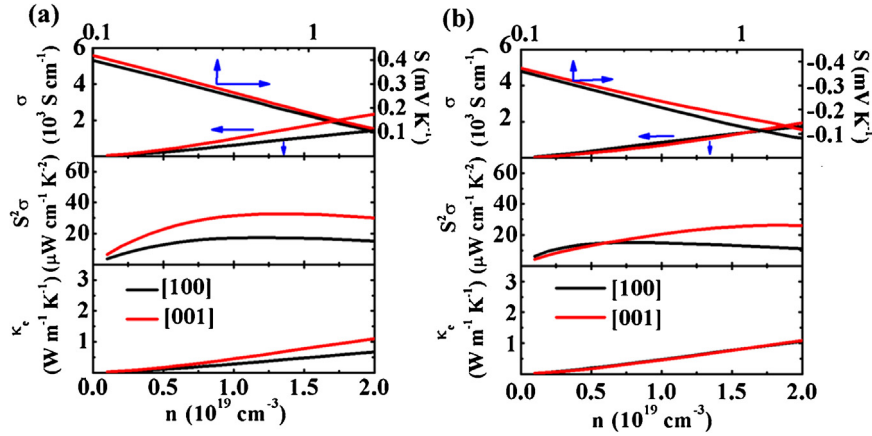


Fig. 2. Electrical conductivity σ , Seebeck coefficient S , power factor $S^2\sigma$, and electronic thermal conductivity κ_e of cubic $\text{CH}_3\text{NH}_3\text{PbI}_3$ at 330K, as a function of hole (a) and electron (b) concentration. The black and red lines represent the [100] and [001] transport directions, respectively. (For interpretation of the references to colour in this figure legend, the reader is referred to the web version of this article.)

As a result, the power factor exhibits a maximum at a certain carrier concentration of c.a. 10^{19} cm^{-3} . In the calculation of charge transport properties, we included two scattering mechanisms of charge carriers, i.e. acoustic phonon scattering and charged impurity scattering. Our previous investigation on intrinsic and extrinsic charge transport in $\text{CH}_3\text{NH}_3\text{PbI}_3$ perovskites showed that at the impurity density of 10^{18} cm^{-3} , the charge carrier mobilities derived at low carrier concentrations were in reasonable agreement with the experimental data reported for $\text{CH}_3\text{NH}_3\text{PbI}_3$ single crystals [26]. In the current study, we therefore set the impurity density to 10^{18} cm^{-3} . The charged impurity scattering is dependent on the carrier concentration through the Debye screening length L_D . For TE applications, the optimal carrier concentration to achieve the largest power factor is on the order of 10^{19} cm^{-3} . The ionized impurity is so screened by free charge carriers at such carrier concentrations that the impurity scattering is substantially weakened and its contribution to charge transport becomes comparable to the acoustic phonon scattering.

According to our previous work [25], when the carrier concentration is not very high the Seebeck coefficient shows a linear relationship with the logarithm of carrier concentration:

$$S = -\frac{k_B}{e} \ln(n) + \frac{k_B}{e} \ln N_{\text{eff}} \quad (10)$$

where N_{eff} is the effective density of states (DOS) near the band edge of valence or conduction bands for holes or electrons. The slope is determined by two physical constants, the Boltzmann constant k_B and the elementary charge e . The intercept is determined by the effective density of states N_{eff} . This linear relationship is well obeyed by our calculation data as clearly seen from Figs. 1 and 2, and the slope is almost the same irrespective of carrier type and crystal phase. Since the effective density of states

near the valence band edge is larger than that near the conduction band edge, the Seebeck coefficient of holes is larger than that of electrons for either cubic or tetragonal phase of $\text{CH}_3\text{NH}_3\text{PbI}_3$. As the magnitude of Seebeck coefficient is related to the DOS, the Seebeck coefficient is isotropic in different transport directions.

The largest power factor at the optimal doping level and the corresponding transport coefficients, including the Seebeck coefficient, the electrical conductivity, the electronic thermal conductivity have been summarized in Table 1. For tetragonal phase, the largest power factor is 53.0 and $30.0 \mu\text{W cm}^{-1} \text{ K}^{-2}$ at the hole concentration of 1.4×10^{19} and $1.2 \times 10^{19} \text{ cm}^{-3}$ in the [100] and [001] directions, respectively, and it is 32.7 and $23.3 \mu\text{W cm}^{-1} \text{ K}^{-2}$ at the electron concentration of 1.0×10^{19} and $8 \times 10^{18} \text{ cm}^{-3}$ in the [100] and [001] directions, respectively. The power factor of holes is larger than electrons in both directions, indicating that tetragonal $\text{CH}_3\text{NH}_3\text{PbI}_3$ is a p-type TE material. The power factor of tetragonal $\text{CH}_3\text{NH}_3\text{PbI}_3$ after doping optimization at 330 K is even comparable to that reported for Na doped SnSe single crystal, which is $\sim 40 \mu\text{W cm}^{-1} \text{ K}^{-2}$ at 300 K and $\sim 14 \mu\text{W cm}^{-1} \text{ K}^{-2}$ at 773 K [6], suggesting tetragonal $\text{CH}_3\text{NH}_3\text{PbI}_3$ is an excellent TE cooling material working in the low-temperature regime. We also find that the power factor in the [100] direction is larger than the [001] direction, which comes from the anisotropy of electrical conductivity. The electrical conductivity of both electrons and holes in cubic phase is smaller than that in tetragonal phase, while the Seebeck coefficient in cubic $\text{CH}_3\text{NH}_3\text{PbI}_3$ is similar to that in tetragonal $\text{CH}_3\text{NH}_3\text{PbI}_3$. As a result, tetragonal phase $\text{CH}_3\text{NH}_3\text{PbI}_3$ shows TE properties superior to cubic phase, with larger power factors for both electrons and holes.

According to the Wiedemann-Franz law $\kappa_e = L\sigma T$, the electronic thermal conductivity exhibits the same trend as the electrical conductivity. L is called the Lorenz constant, which takes the

Table 1
TE transport properties of $\text{CH}_3\text{NH}_3\text{PbI}_3$ perovskite at the optimal doping level and the phase transition temperature.

	Direction	Carrier density (10^{19} cm^{-3})	S ($\mu\text{V K}^{-1}$)	σ (10^3 S cm^{-1})	$S^2\sigma$ ($\mu\text{W cm}^{-1} \text{ K}^{-2}$)	κ_e ($\text{W m}^{-1} \text{ K}^{-1}$)	L/L_0
Tetragonal	h	[100]	135	2.89	53.0	1.53	0.67
		[001]	142	1.48	30.0	0.71	0.60
	e	[100]	-130	1.92	32.7	1.04	0.67
		[001]	-143	1.15	23.3	0.62	0.66
Cubic	h	[100]	150	0.78	17.5	0.36	0.57
		[001]	147	1.53	32.8	0.71	0.57
	e	[100]	-153	0.65	15.2	0.35	0.65
		[001]	-126	1.66	26.2	0.96	0.71

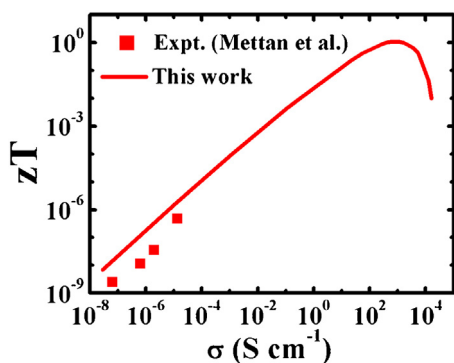


Fig. 3. zT as a function of electrical conductivity σ for p-type tetragonal $\text{CH}_3\text{NH}_3\text{PbI}_3$ in comparison with the available experimental data of Ref. [21] at the experimental temperature of 295 K. The calculation result shown is along the [100] direction.

Sommerfeld theoretical value L_0 of $2.44 \times 10^{-8} \text{ W } \Omega \text{ K}^{-2}$ for free electrons. We noted that at the optimal carrier concentration, the Lorenz factor is reduced by about 30–40% with respect to the Sommerfeld value L_0 . In our previous investigations of TE materials, either organic or inorganic, we constantly observed such a drop of the Lorenz factor at the optimal doping level compared to the theoretical value for free electrons [24,36,37]. When the carrier concentration is very high, such as in heavily doped PEDOT:Tos we studied previously, the Lorenz number is approaching the theoretical value since such heavily doped systems already show the metallic behavior [24]. In some experimental and theoretical investigations, the electronic thermal conductivity is obtained by directly applying the Wiedemann-Franz law to the electrical conductivity, which is usually easily derived both experimentally and theoretically. In such cases, the correction to the Sommerfeld value is suggested using a scaling factor of 60–70%, according to our calculations.

To achieve a high TE figure of merit, organic-inorganic hybrid perovskites have to be poor thermal conductors. The lattice thermal conductivity of orthorhombic and tetragonal $\text{CH}_3\text{NH}_3\text{PbI}_3$ has been experimentally measured [19], and that of tetragonal and cubic phases has been theoretically derived [20]. Good agreement between experimental and theoretical data has been established for tetragonal phase of $\text{CH}_3\text{NH}_3\text{PbI}_3$. Based on these data, we can derive the zT value of perovskite. Fig. 3 shows the zT value of p-type tetragonal $\text{CH}_3\text{NH}_3\text{PbI}_3$ as a function of the electrical conductivity at 295 K. The lattice thermal conductivity of $0.59 \text{ W m}^{-1} \text{ K}^{-1}$ is adopted according to Ref. [20]. At low carrier concentrations, the zT values agree well with the experimental data measured at the same temperature by photo doping [21]. In the photo doping, the free carrier density was estimated to be only

10^{14} cm^{-3} [21]. Obviously, this carrier concentration is insufficient for the optimal TE performance. Our data show that zT of hole-doped tetragonal $\text{CH}_3\text{NH}_3\text{PbI}_3$ can be as high as one if the carrier concentration is accurately tuned towards the optimal level. Although photo-excitation is unable to generate sufficient charge carriers for efficient TE conversion, Mettan et al. predicted that the zT value can be enhanced to one by increasing electrical conductivity via chemical doping [21]. Our theoretical calculations confirmed this. The maximum zT value for p-type $\text{CH}_3\text{NH}_3\text{PbI}_3$ at 295 K is calculated to be 1.08 when the electrical conductivity is enhanced to $\sim 900 \text{ S cm}^{-1}$, and the corresponding carrier concentration is $6 \times 10^{18} \text{ cm}^{-3}$, four orders of magnitude higher than the photo-generated carrier concentration.

The theoretical calculations by Qian et al. [20] have provided the lattice thermal conductivity of $\text{CH}_3\text{NH}_3\text{PbI}_3$ spanning a temperature range from 150 K to 400 K. Fig. 4a shows their results on the temperature dependence of lattice thermal conductivity. There is an abrupt increase of the thermal conductivity when $\text{CH}_3\text{NH}_3\text{PbI}_3$ transits from tetragonal to cubic phase, which has been explained by the higher phonon group velocity and lower anharmonicity in cubic $\text{CH}_3\text{NH}_3\text{PbI}_3$ [20]. In either phase, the lattice thermal conductivity decreases as the temperature increases. Low thermal conductivity favors high TE efficiency. Fig. 4b shows our predictions of the largest value of zT and the corresponding carrier concentration as a function of temperature, based on the lattice thermal conductivity derived by Qian et al. [20]. As shown above the power factor of tetragonal phase is larger than that of cubic phase, and the lattice thermal conductivity increases abruptly when going from tetragonal to cubic phase, the zT value exhibits an abrupt drop at the phase transition temperature. Moreover, the zT value in both tetragonal and cubic $\text{CH}_3\text{NH}_3\text{PbI}_3$ increases with the increasing temperature. So the best TE performance is observed in tetragonal $\text{CH}_3\text{NH}_3\text{PbI}_3$ at the phase transition point, with the zT value of 1.26. This value is very high for bulk TE materials, even comparable to the high-performing nanostructured bismuth antimony telluride bulk alloys, which have a zT value about 1.2 at room temperature [38].

3.2. Hole-doping site for efficient TE conversion

In the above, we have demonstrated the importance of tuning carrier concentration for the best TE performance. In our calculations, we assumed that doping has little influence on the band structure of host materials if the dopant concentration is low. Since tetragonal $\text{CH}_3\text{NH}_3\text{PbI}_3$ has exhibited excellent p-type TE properties when optimally doped, we hope to find a way to tune the hole concentration while minimally alter its band structure. To shed light on the potential hole-doping sites in tetragonal

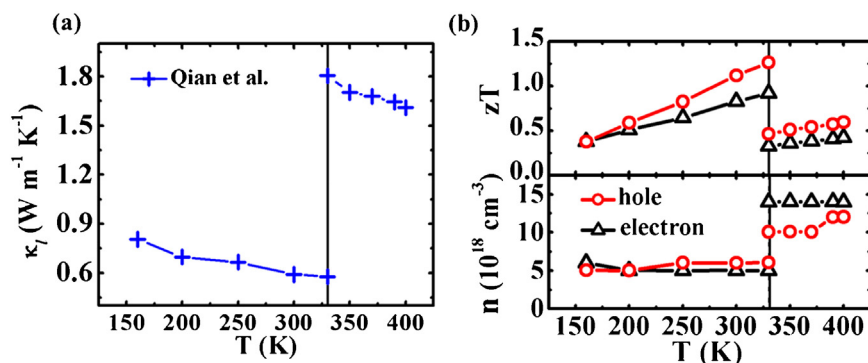


Fig. 4. (a) Temperature dependence of the lattice thermal conductivity κ_l reproduced from the theoretical work of Qian et al. [20]. (b) Maximum zT and the corresponding optimal carrier concentration as a function of temperature for holes (red) and electrons (black) in the [100] direction. (For interpretation of the references to colour in this figure legend, the reader is referred to the web version of this article.)

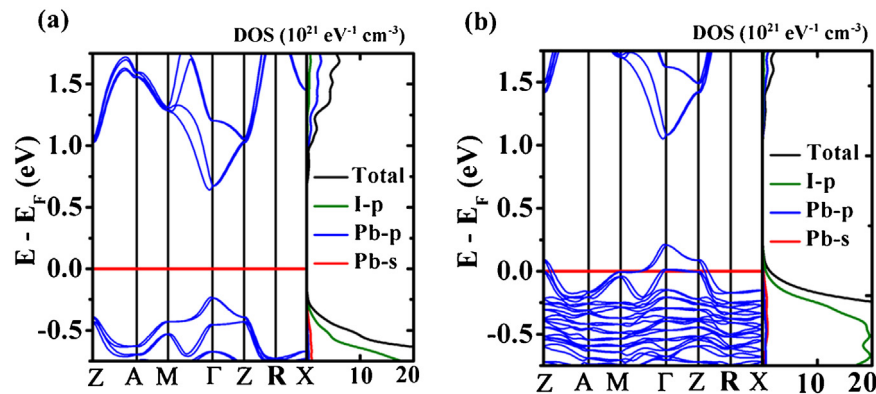


Fig. 5. Electronic band structure and partial density of states (PDOS) for (a) perfect tetragonal $\text{CH}_3\text{NH}_3\text{PbI}_3$ and (b) tetragonal $\text{CH}_3\text{NH}_3\text{PbI}_3$ with one CH_3NH_3 vacancy in a unit cell.

$\text{CH}_3\text{NH}_3\text{PbI}_3$, we analyzed its band structure and partial DOS (Fig. 5a). The valence band of $\text{CH}_3\text{NH}_3\text{PbI}_3$ is composed of I-5p atomic orbital and Pb-6s atomic orbital. The orbitals of methylammonium cations do not contribute to the frontier orbitals. We then expect that vacancies of organic cations will give rise to holes in such organic-inorganic hybrid perovskites, without altering the band structure. As a demonstration, we calculated the band structure of tetragonal $\text{CH}_3\text{NH}_3\text{PbI}_3$ with one organic cation missing in the unit cell (Fig. 5b). As compared to the perfect crystal, the valence band structure of defect crystal is barely changed, only the Fermi level has shifted into the valence band. There exist four organic cations in one unit cell, with one organic cation missing, the vacancy concentration will be on the order of 10^{20} cm^{-3} , so the hole concentration is on the same order of magnitude. This hole concentration is one order of magnitude higher than the optimal doping level, to achieve the optimal carrier concentration we need one organic cation vacancy in ten unit cells of tetragonal $\text{CH}_3\text{NH}_3\text{PbI}_3$. In other words, by engineering the vacancy of organic anions in tetragonal $\text{CH}_3\text{NH}_3\text{PbI}_3$, we can significantly improve its TE efficiency. The silver doping have been shown to enhance the electrical conductivity of the CdI_2 -type PbI_2 polymer sheet β -(EDT-TTF- I_2) $_2$ [$\text{Pb}_{2/3+x}\text{Ag}_{1/3-2x}\text{I}_x$] $_3$, $x = 0.05$ [39]. By substitution at the Pb-site with Ag, we can also realize p-doping in $\text{CH}_3\text{NH}_3\text{PbI}_3$. However, in this case the band structure will be modified since the Pb-6s contributed to the valence band. Based on these calculations, we propose to dope optimization of $\text{CH}_3\text{NH}_3\text{PbI}_3$ by engineering vacancies of organic cations for high TE efficiency.

4. Conclusions

It should be noted that there has been tremendous progresses made in the past decades in the advances in electronic structure theory [40]. Computational evaluation of optoelectronic property for materials becomes realistic [41]. We have studied the TE transport properties of both tetragonal and cubic phases of $\text{CH}_3\text{NH}_3\text{PbI}_3$ perovskite by combining the first-principles electronic structure calculations and the Boltzmann transport equation. We find that tetragonal $\text{CH}_3\text{NH}_3\text{PbI}_3$ has superior TE properties than cubic one, and its zT value is the highest at the phase transition temperature of 330 K, exceeding one when the accurate hole-doping can be achieved. The optimal doping level is on the order of 10^{18} – 10^{19} cm^{-3} . Our results suggest that tetragonal $\text{CH}_3\text{NH}_3\text{PbI}_3$ is a promising p-type TE cooling material in the low-temperature regime. We also propose that $\text{CH}_3\text{NH}_3\text{PbI}_3$ can be hole-doped by

engineering vacancies of organic cations, without modifying the electronic structure near the valence band edge.

Acknowledgements

This work is supported by the National Natural Science Foundation of China (Grant nos. 21273124, 21673123, 21290190, and 91333202) and the Ministry of Science and Technology of China (Grant nos. 2013CB933503 and 2015CB655002). Computational resources are provided by the Tsinghua Supercomputing Center.

References

- [1] A.J. Minnich, M.S. Dresselhaus, Z.F. Ren, G. Chen, Bulk nanostructured thermoelectric materials: current research and future prospects, *Energy Environ. Sci.* 2 (2009) 466–479.
- [2] D. Wang, W. Shi, J. Chen, J. Xi, Z. Shuai, Modeling thermoelectric transport in organic materials, *Phys. Chem. Chem. Phys.* 14 (2012) 16505–16520.
- [3] W.G. Zeier, A. Zevalkink, Z.M. Gibbs, G. Hautier, M.G. Kanatzidis, G.J. Snyder, Thinking like a chemist: intuition in thermoelectric materials, *Angew. Chem. Int. Ed. Engl.* 55 (2016) 6826–6841.
- [4] J.P. Heremans, M.S. Dresselhaus, L.E. Bell, D.T. Morelli, When thermoelectrics reached the nanoscale, *Nat. Nanotechnol.* 8 (2013) 471–473.
- [5] L.-D. Zhao, V.P. Dravid, M.G. Kanatzidis, The panoscopic approach to high performance thermoelectrics, *Energy Environ. Sci.* 7 (2014) 251–268.
- [6] L.-D. Zhao, G. Tan, S. Hao, J. He, Y. Pei, H. Chi, H. Wang, S. Gong, H. Xu, V.P. Dravid, C. Uher, G.J. Snyder, C. Wolverton, M.G. Kanatzidis, Ultrahigh power factor and thermoelectric performance in hole-doped single-crystal SnSe , *Science* 351 (2016) 141–144.
- [7] L.E. Bell, Cooling, heating, generating power, and recovering waste heat with thermoelectric systems, *Science* 321 (2008) 1457–1461.
- [8] G.-H. Kim, L. Shao, K. Zhang, K.P. Pipe, Engineered doping of organic semiconductors for enhanced thermoelectric efficiency, *Nat. Mater.* 12 (2013) 719–723.
- [9] O. Bubnova, Z.U. Khan, H. Wang, S. Braum, D.R. Evans, M. Fabretto, P. Hojati-Talemi, D. Dagnelund, J.B. Arlin, Y.H. Geerts, S. Desbief, D.W. Breiby, J.W. Andreasen, R. Lazzaroni, W.M. Chen, I. Zozoulenko, M. Fahlman, P.J. Murphy, M. Berggren, X. Crispin, Semi-metallic polymers, *Nat. Mater.* 13 (2014) 190–194.
- [10] Y. Sun, L. Qiu, L. Tang, H. Geng, H. Wang, F. Zhang, D. Huang, W. Xu, P. Yue, Y.S. Guan, F. Jiao, Y. Sun, D. Tang, C.A. Di, Y. Yi, D. Zhu, Flexible n-type high-performance thermoelectric thin films of poly(nickel-ethylenetetrathiolate) prepared by an electrochemical method, *Adv. Mater.* 28 (2016) 3351–3358.
- [11] C. Wan, X. Gu, F. Dang, T. Itoh, Y. Wang, H. Sasaki, M. Kondo, K. Koga, K. Yabuki, G.J. Snyder, R. Yang, K. Koumoto, Flexible n-type thermoelectric materials by organic intercalation of layered transition metal dichalcogenide TiS_2 , *Nat. Mater.* 14 (2015) 622–627.
- [12] A. Kojima, K. Teshima, Y. Shirai, T. Miyasaka, Organometal halide perovskite as visible-light sensitizers for photovoltaic cells, *J. Am. Chem. Soc.* 131 (2009) 6050–6051.
- [13] M. Liu, M.B. Johnston, H.J. Snaith, Efficient planar heterojunction perovskite solar cells by vapour deposition, *Nature* 501 (2013) 395–398.
- [14] http://www.nrel.gov/pv/assets/images/efficiency_chart.jpg, 6th December 2016.
- [15] J. You, L. Meng, T.B. Song, T.F. Guo, Y.M. Yang, W.H. Chang, Z. Hong, H. Chen, H. Zhou, Q. Chen, Y. Liu, N. De Marco, Y. Yang, Improved air stability of perovskite

- solar cells via solution-processed metal oxide transport layers, *Nat. Nanotechnol.* 11 (2016) 75–81.
- [16] G.D. Niu, X.D. Guo, L.D. Wang, Review of recent progress in chemical stability of perovskite solar cells, *J. Mater. Chem. A* 3 (2015) 8970–8980.
- [17] G. Niu, W. Li, F. Meng, L. Wang, H. Dong, Y. Qiu, Study on the stability of $\text{CH}_3\text{NH}_3\text{PbI}_3$ films and the effect of post-modification by aluminum oxide in all-solid-state hybrid solar cells, *J. Mater. Chem. A* 2 (2014) 705–710.
- [18] I. Hwang, I. Jeong, J. Lee, M.J. Ko, K. Yong, Enhancing stability of perovskite solar cells to moisture by the facile hydrophobic passivation, *ACS Appl. Mater. Interfaces* 7 (2015) 17330–17336.
- [19] A. Pisoni, J. Jacimovic, O.S. Barisic, M. Spina, R. Gaal, L. Forro, E. Horvath, Ultra-low thermal conductivity in organic-inorganic hybrid perovskite $\text{CH}_3\text{NH}_3\text{PbI}_3$, *J. Phys. Chem. Lett.* 5 (2014) 2488–2492.
- [20] X. Qian, X. Gu, R. Yang, Lattice thermal conductivity of organic-inorganic hybrid perovskite $\text{CH}_3\text{NH}_3\text{PbI}_3$, *Appl. Phys. Lett.* 108 (2016) 063902.
- [21] X. Mettan, R. Pisoni, P. Matus, A. Pisoni, J. Jaćimović, B. Náfrádi, M. Spina, D. Pavuna, L. Forró, E. Horváth, Tuning of the thermoelectric figure of merit of $\text{CH}_3\text{NH}_3\text{MI}_3$ (M = Pb, Sn) photovoltaic perovskites, *J. Phys. Chem. C* 119 (2015) 11506–11510.
- [22] Y. He, G. Galli, Perovskites for solar thermoelectric applications: a first principle study of $\text{CH}_3\text{NH}_3\text{Al}_3$ (A = Pb and Sn), *Chem. Mater.* 26 (2014) 5394–5400.
- [23] C. Lee, J. Hong, A. Stroppa, M.-H. Whangbo, J.H. Shim, Organic-inorganic hybrid perovskites ABI_3 (A = CH_3NH_3 , NH_2CHNH_2 ; B = Sn, Pb) as potential thermoelectric materials: a density functional evaluation, *RSC Adv.* 5 (2015) 78701.
- [24] W. Shi, T. Zhao, J. Xi, D. Wang, Z. Shuai, Unravelling doping effects on PEDOT at the molecular level: from geometry to thermoelectric transport properties, *J. Am. Chem. Soc.* 137 (2015) 12929–12938.
- [25] W. Shi, J. Chen, J. Xi, D. Wang, Z. Shuai, Search for organic thermoelectric materials with high mobility: the case of 2,7-dialkyl[1]benzothieno[3,2-b][1]benzothiophene derivatives, *Chem. Mater.* 26 (2014) 2669–2677.
- [26] T. Zhao, W. Shi, J. Xi, D. Wang, Z. Shuai, Intrinsic and extrinsic charge transport in $\text{CH}_3\text{NH}_3\text{PbI}_3$ perovskites predicted from first-principles, *Sci. Rep.* 7 (2016) 19968.
- [27] G. Kresse, J. Furthmuller, Efficiency of ab-initio total energy calculations for metals and semiconductors using a plane-wave basis set, *Comput. Mater. Sci.* 6 (1996) 15–50.
- [28] G. Kresse, J. Furthmuller, Efficient iterative schemes for ab initio total-energy calculations using a plane-wave basis set, *Phys. Rev. B* 54 (1996) 11169–11186.
- [29] J.P. Perdew, K. Burke, M. Ernzerhof, Generalized gradient approximation made simple, *Phys. Rev. Lett.* 77 (1996) 3865–3868.
- [30] G.K.H. Madsen, D.J. Singh, BoltzTraP. A code for calculating band-structure dependent quantities, *Comput. Phys. Commun.* 175 (2006) 67–71.
- [31] J. Bardeen, W. Shockley, Deformation potentials and mobilities in non-polar crystals, *Phys. Rev.* 80 (1950) 72–80.
- [32] J. Xi, M. Long, L. Tang, D. Wang, Z. Shuai, First-principles prediction of charge mobility in carbon and organic nanomaterials, *Nanoscale* 4 (2012) 4348–4369.
- [33] D. Chattopadhyay, H.J. Queisser, Electron scattering by ionized impurities in semiconductors, *Rev. Mod. Phys.* 53 (1981) 745–768.
- [34] M. Hirasawa, T. Ishihara, T. Goto, K. Uchida, N. Miura, Magnetoabsorption of the lowest excitation in perovskite-type compound $(\text{CH}_3\text{NH}_3)\text{PbI}_3$, *Phys. B* 201 (1994) 427–430.
- [35] G. Zhou, D. Wang, High thermoelectric performance from optimization of hole-doped CuInTe_2 , *Phys. Chem. Chem. Phys.* 18 (2016) 5925–5931.
- [36] G. Zhou, D. Wang, Few-quintuple Bi_2Te_3 nanofilms as potential thermoelectric materials, *Sci. Rep.* 5 (2015) 8099.
- [37] J. Chen, D. Wang, Z. Shuai, First-principles predictions of thermoelectric figure of merit for organic materials: deformation potential approximation, *J. Chem. Theory Comput.* 8 (2012) 3338–3347.
- [38] B. Poudel, Q. Hao, Y. Ma, L. Yucheng, A. Minnich, B. Yu, X. Yan, D. Wang, A. Muto, D. Vashaee, X. Chen, J. Liu, M.S. Dresselhaus, G. Chen, Z. Ren, High-thermoelectric performance of nanostructured bismuth antimony telluride bulk alloys, *Science* 320 (2008) 634–638.
- [39] T. Devic, M. Evain, Y. Moelo, E. Canadell, P. Auban-Senzier, M. Fourmigue, P. Batail, Single crystalline commensurate metallic assemblages of π -slabs and CdI_2 -type layers: synthesis and properties of β -(EDT-TTF- I_2) $_2$ [$\text{Pb}_{5/6}\square_{1/6}\text{I}_2$] $_3$ and β -(EDT-TTF- I_2) $_2$ [$\text{Pb}_{2/3+x}\text{Ag}_{1/3-2x}\square_x\text{I}_2$] $_3$, $x=0.05$, *J. Am. Chem. Soc.* 125 (2003) 3295–3301.
- [40] E. Clementi, Evolution of computers and simulations: from science and technology to the foundations of society, *Sci. China Chem.* 57 (2014) 1317–1329.
- [41] Z. Shuai, D. Wang, Q. Peng, H. Geng, Computational evaluation of optoelectronic properties for organic/carbon materials, *Acc. Chem. Res.* 47 (2014) 3301–3309.